Cassini observations of aperiodic waves on Saturn's magnetodisc

C. J. Martin[1], **C. S. Arridge**[1]

[1]Physics Department, Lancaster University, Bailrigg, Lancaster, LA1 4YB, United Kingdom.

Key Points:

- Saturn's current sheet is distorted by many aperiodic waves in all local time sectors
- The properties of these aperiodic waves can be found by deforming a current sheet model with a Gaussian wave pulse
- Waves predominantly propagate radially outwards on a thickening current sheet with increasing amplitude with radial distance

Corresponding author: C. J. Martin , c.martin1@lancaster.ac.uk

Abstract

The location and motion of Saturn's equatorial current sheet is the result of an interplay between a quasi-static deformation that varies in radial distance and local time, impulsive perturbations that produce large-scale displacements, quasi-periodic perturbations near the planetary rotation period, and wave-like structures on shorter timescales. This study focuses on the latter, aperiodic wave pulses with periods from 1-30 minutes, that are unrelated to the quasi-periodic 'flapping' with a period near that of Saturn's rotation. Cassini magnetometer data were surveyed for these aperiodic structures and then fitted to a simple model in order to estimate the properties of the waves.The model consists of a modified Harris current sheet model deformed by a Gaussian pulse wave function. This then allows for the extraction of wave parameters and current sheet properties. In particular we show an increase in current sheet scale height with radial distance from Saturn, an increase in the wave amplitude with radial distance, and the resolution of propagation directions using the wave vector fitted by the model. The dominant propagation direction is found to be radially outwards from Saturn.

1 Introduction

Saturn's magnetosphere is, to an important extent, rotationally driven [*Southwood et al.*, 2001] and contains internal plasma sourced from the moon Enceladus and to a lesser extent the rings, other satellites and the planet itself [e.g. *Pontius et al.* [2006], *Tokar et al.* [2005], *Jurac et al.* [2002] & *Felici et al.* [2016]] .The magnetosphere outside of $20R_S$ (Saturn radii) is dominated by the magnetodisc current sheet, a washer shaped sheet of particles caused, in part, by the centrifugal stresses of the fast-rotating magnetosphere [*Arridge et al.*, 2007]. Although other particle stresses are imparted, the disc-like current sheet forms at the point that centrifugal stresses dominate over magnetic tension and pressure gradients, which occurs at $\sim 15R_S$, and extends to the magnetopause. This azimuthal current sheet causes the magnetic field of Saturn to appear radially distended, similar to that of Jupiter's middle and outer magnetosphere.

Additionally, the azimuthal magnetic field structure is affected by rotation and solar wind compression. At large radial distances, magnetic field lines are 'swept back' due to plasma sub-corotation, causing an increasing azimuthal field component with radial distance. However, on the dusk sector of the magnetosphere, the confinement from the solar wind causes a 'swept forward' field that is pushed forward in the direction of co-rotation.

Dynamic pressure of the solar wind acting on the dayside magnetosphere also plays a role on the structure of the azimuthal field. Under higher solar wind dynamic pressures, the dayside will be more compressed, moving the region of corotation breakdown closer to the magnetopause and leading to a more corotating dayside with less swept-back field lines, or swept-forward field lines on the dusk flank due to the effect of the Chapman-Ferarro currents. Under transient solar wind compressions the dayside magnetosphere might undergo a short period of super-corotation which may produce swept-forward field lines in the noon sector [e.g. *Southwood et al.* [2001]]. Saturn's equatorial current sheet has been found in all local time sectors, however the dayside magnetosphere sometimes exhibits no ordered current sheet structure when the magnetosphere is compressed [*Arridge et al.*, 2008b].

Many processes cause the current sheet to be displaced from the rotational equator. Seasonal differences combined with the influence of solar wind pressure [*Arridge et al.*, 2008a] will cause the current sheet to be pushed above the rotational equator in Northern winter time and pushed below the equator in Northern summer time, hence forming a 'bowl shape'. Hence, if Cassini is in the same position for a Saturnian year, the magnetometer will read one wavelength of the current sheet bowl movement. Therefore, Saturn's current sheet experiences a periodic wave with a time period of 30 years. Seasonal changes also affect the current sheet thickness, *Sergis et al.* [2011] has shown that the current sheet thickness will be highly variable during the seasons and even between subsequent orbits, and will exhibit north-south asymmetries in the thickness of plasma. Temperature, density and pressure, however, remain unchanged.

Another periodicity apparent in the magnetometer data is the ~10.7 hour rotation rate flapping motion [*Arridge et al.* [2011] & *Provan et al.* [2012]]. The origin of this flapping motions is thought to be caused by rotating magnetic perturbations in each hemisphere [e.g. *Arridge et al.* [2008a], *Andrews et al.* [2010], *Jia and Kivelson* [2012]]. This flapping motion is also thought to superpose with thickness variations of the current sheet as it propagates [*Thomsen et al.*, 2016].

The focus of this study is the much shorter timescale, aperiodic waves that occur in addition to the waves discussed previously. These waves occur over time periods of 1-30 minutes and appear in all areas where a current sheet is present but do not repeat periodically or show a sinusoidal period. The time period refers to the length of time that the wave is detected. *Arridge et al.* [2007] previously used these waves to calculate the stress balance in Saturn's magnetosphere but their origins or properties are yet to be explored. These features also occur frequently in Earth's magnetotail current sheet [*Sergeev et al.*, 2004] and have been seen on Jupiter's magnetodisc [*Russell et al.*, 1999]. They were also present in Pioneer 11 magnetometer data at Saturn [*Smith et al.*, 1980]. Cassini's varied orbital trajectory and spatial coverage give an unique opportunity for studying these waves on a large scale.

Small-amplitude periodicities and fluctuations are also present within Saturn's magnetosphere, an example of such are the quasi-periodic waves discussed within *Mitchell et al.* [2016], *Palmaerts et al.* [2016] & *Yates et al.* [2016] where the authors present quasi-hourly pulsations in UV auroral observations along with particle and magnetic field data. These waves appear similar to the waves presented within this study, however only waves that are singular and non-repeating are included within the study. Similar structures are also found in the jovian magnetosphere [*Khurana and Kivelson*, 1989]. *von Papen et al.* [2014] & *von Papen & Saur* [2016] discuss fluctuations and magnetic turbulence within the middle magnetosphere. These studies measure fluctuations in the magnetometer data in 10 minute bins, where the spacial range of *von Papen & Saur* [2016] overlaps with the spacial range of this study, it is possible that the aperiodic waves we discuss in this paper fall within the fluctuations of the current sheet shown in *von Papen & Saur* [2016] at the inner bound of this study.

2 Magnetometer Data

We use Cassini's onboard fluxgate magnetometer [*Dougherty et al.*, 2004] to detect the signatures of aperiodic waves using data with a time resolution of 1 Hz. Magnetometer data and the following model are presented in spherical KRTP coordinates (Kronian radial, theta, phi) where the first component, $\hat{\boldsymbol{r}}$, is from the centre of Saturn radially outwards. $\hat{\boldsymbol{\theta}}$ is positive Southward at the equator, and $\hat{\boldsymbol{\phi}}$ is positive in the direction of co-rotation. Additionally, a Cartesian local coordinate system $(\boldsymbol{x}, \boldsymbol{y}, \boldsymbol{z})$ is used when forming the model and fitting to it. This system gives $\hat{\boldsymbol{x}}$ in the radial direction, $\hat{\boldsymbol{y}}$ in the direction of co-rotation, this is assumed as Cartesian in the local system, and $\hat{\boldsymbol{z}}$ is equivalent to $-\hat{\theta}$ at the equator in the spherical polar system. All results are converted back to spherical polar coordinates. Furthermore, the KSM (Kronocentric Solar Magnetospheric) ($\hat{\boldsymbol{X}}$,$\hat{\boldsymbol{Y}}$,$\hat{\boldsymbol{Z}}$) system is useful in interpretation. Where $\hat{\boldsymbol{X}}$ is the vector pointing to the Sun, $\hat{\boldsymbol{Y}}$ is perpendicular to the rotation axis towards dusk and $\hat{\boldsymbol{Z}}$ is northwards so that the rotation axis is in the X-Z plane.

Aperiodic waves have a distinct signature in magnetic field data. As an aperiodic wave passes Cassini we find that the B_r and B_ϕ components have an anti-phase relationship due to the largely swept backwards nature of the field lines. During the passage of an aperiodic wave Cassini will be embedded in either lobe of the magnetosphere and as the wave passes, the spacecraft will sample the current sheet, the opposing lobe (if the wave has sufficient amplitude), the current sheet again, and finally the original lobe.

As Saturn's magnetic field at distances of larger than $20R_S$ is mainly radial with a small contribution from the azimuthal component, the magnetometer data will see the passing of a wave in the radial component. If Cassini is originally in the Southern lobe B_r will be negative and will increase through zero as Cassini traverses the centre of the current sheet to positive B_r in the Northern lobe. The radial component will then decrease from a maximum back to the starting value, again crossing zero as Cassini crosses the current sheet centre. The azimuthal component follows a similar profile, but with an opposite polarity when the field is swept-back. So starting in the Southern lobe, B_ϕ would be positive and would decrease through zero to a negative value when a maximum positive value is reached in B_r. This signature is shown in figure 1.

The third magnetic field component, B_θ varies depending on various other processes. As $\hat{\theta}$ is positive Southward at the equator, this means that with no external processes occurring B_θ will be a constant positive. However, during the passage of an aperiodic wave, the θ component may show deviations that differ depending on the parameters of the wave that is distorting the current sheet. Figure 1 shows magnetic field signatures of a solely radially propagating wave and a solely azimuthally propagating wave. Many examples show a mixture of radial and azimuthal propagation along with various other processes, such as dipolarization and guide fields, that affect the θ component.

These aperiodic waves are detected by their distinct characteristics. We select field perturbations that have a smaller time period than the global flapping waves, are non-repeating, and show a deflection in the radial magnetic field of over 1nT. The event must also occur inside of the magnetopause position found by an examination of the magnetic field data. In total, 1461 events fit these criteria from all revolutions of Cassini that occur between $\pm 10R_S$ of the rotational equator from January 2005 to December 2012.

3 Current Sheet Model

To determine the propagation and properties of a wave on a current sheet from single spacecraft measurements we use a simple local current sheet model. We require a model that includes the variation of radial magnetic field from positive above the equator to negative below the equator. Hence, a Harris current sheet model [*Harris*, 1962] is used for the radial component of the magnetic field, given in equation 1. Equation 2 is used for the azimuthal field component, where if the field is swept backwards we will see a negative B_{y0}, and where the field is swept forward we have a positive B_{y0}. The third and final magnetic field component, the component normal to the current sheet, is modelled as a constant. Deformation of the current sheet will generate a non-constant B_z (Equation 3). This model is true solely at close proximity to the current sheet and outside of the dipolar region of Saturn's magnetosphere. The model also relies on the thin sheet approximation [*Vasyliunas*, 1983]. Because of these reasons the model is presented in Cartesian local coordinates (x, y, z).

$$B_x = B_{x0} \tanh\left(\frac{z - z_0}{H_x}\right) \tag{1}$$

$$B_y = B_{y0} \tanh\left(\frac{z - z_0}{H_y}\right) \tag{2}$$

$$B_z = B_{z0} \tag{3}$$

B_{x0}, B_{y0} and B_{z0} are lobe values (or asymptotic value of the hyperbolic tangent function). The sign of B_{y0} is related to the sweep-back and sweep-forward of the magnetic field. A negative value of B_{y0} means that below the current sheet B_y will be positive and above the current sheet B_y will be negative and the field will be swept backwards if we assume B_x is positive above the sheet and negative below. The converse applies if B_{y0} is positive. The current sheet scale height, or how quickly the hyperbolic tangent function reaches its asymptotic value, is given by H_x and H_y. The displacement of the current sheet from the rotational equator, for example by the global flapping and bowl shape, is included through the z_0 parameter. These parameters all describe the local properties of the current sheet, all distances are fitted in units of Saturn radii and all magnetic field quantities in units of nT.

This local model of the magnetic field must then be deformed by a wave. We use a Gaussian pulse wave function as it describes a singular non-repeating wave which can be easily modified to fit magnetometer data. Equation 4 describes the displacement of the current sheet as $z(x, y, t)$ from z=0.

$$z = A \exp\left[-(\mathbf{k}\cdot\mathbf{r} + \mathbf{k}\cdot\mathbf{u}t - \omega t - \Phi_0)^2\right] \tag{4}$$

Where A is the amplitude of the wave, $\mathbf{k}$ is the wave vector, $\mathbf{k}\cdot\mathbf{u}t$ is the Doppler shift due to the movement of plasma, ω is the angular frequency and Φ_0 is the phase of the wave.

We now have the static current sheet model and a wave to deform it. The deformation of the current sheet is carried out using the general deformation method found in *Tsyganenko* [1998]. This method is ideal as it uses Euler potentials to find the deformed coordinate system whilst keeping the field divergence free, but requires no knowledge of what the Euler potentials are.

Firstly, we need to evaluate the magnetic field in a co-ordinate system that has been deformed by the wave function. This is done by finding the normal to the wave, using the differentials of the original wave function in x and y. This normal can then be used to find the new radial (X) axis and azimuthal (Y) axis using cross products to retain a right-handed system. Now we can find the positions in the new coordinate system, which are then put into the Harris current sheet equation with initial estimates of scale heights and lobe values to find the magnetic field components in the new coordinate system ($\mathbf{B}^*$).

$$\mathbf{B}' = \hat{\mathbf{T}}\mathbf{B}^* \tag{5}$$

The general deformation method is then used to deform this magnetic field using Equations 6 in *Tsyganenko* [1998]. The matrix these equations form, $\hat{\mathbf{T}}$, can then be used to find the final deformed magnetic field components using equation 5. Since the coordinate system is a local current sheet system based on the current sheet normal vector, these derivatives are found using centred finite differences. B^* denotes the magnetic field in the new coordinate system and B' shows the new deformed magnetic field.

With reasonable initial guesses, this local model of the current sheet deformed by a Gaussian wave function can model accurately the changes of a magnetic field during the passage of an aperiodic wave shown in figures 2 and 3.

4 Fitting Magnetometer Data to Model

The local current sheet model has 11 free parameters; six parameters describing the undisturbed planar current sheet (B_{x0}, B_{y0}, B_{z0}, H_x, H_y, z_0) from equations (1,3), and five parameters describing the properties of the wave (k_x, k_y, ω, Φ_0, A) from equation (4)

Due to the large number of variables that require fitting and the possible interdependence of the variables (for example, a negative scale height arising in y from the fact that the lobe magnetic field B_{y0} should be negative instead), an iterative process is used which fits half the variables using a Levenberg-Marquardt nonlinear least squared fitting algorithm with the other variables held constant, and then vice versa. The variables are treated in two distinct groups (B_{y0}, H_y, k_x, k_y and A) and (B_{x0}, B_{z0}, H_x, ω, and z_0). Changing the order of the group that fits first and second has no effect on the final fit, however changing which variables are in each group does change the result.

The groups given previously were used as they return the most fits with the lowest mean squared error (MSE) of the fit, identified by trial and improvement. The process of fitting half and holding constant the remaining variables repeats until the MSE of the fitting is below a threshold of 0.1 nT^2 as during testing, fits with below this values were more likely to be considered good. This process is then iterated over to find the phase, Φ_0, between $0 - 2\pi$ that gives the lowest MSE, and hence the most accurate fitting. This entire algorithm is then run four times with a different combination of positive and negative wave numbers as initial guesses to reduce any bias in wave number selection. The remaining values for initial guesses were taken from preliminary experiments that tested the sensitivity and ability of the algorithm to fit the different parameters. The run with the smallest MSE will be the final selected fitting giving the values of the 11 parameters.

In total, 793 out of 1461 wave events can be fitted using this method. This number of events being fitted is expected as many events exhibit multiple crossings of the current sheet leading to the conclusion that other processes are occurring at the same time or multiple waves are superposed during the event time window, and hence cannot be fitted by just one wave function. Some events, although they fit the criteria of selection, on further inspection do not follow the general signature of a wave but that of an O- or X-line traversal. These are easily filtered out as the local model will not fit the data well as the B_θ component of magnetic field will change sign rapidly and then remain constant at the new value throughout the time frame. Additionally, each fitting is associated with a MSE result of how well the model fits the magnetometer data as well as each event being manually inspected to confirm a correct fitting has occurred.

All fitting is done in Cartesian local coordinates, so magnetometer data is converted to Cartesian before the fitting procedure, but to be in line with convention both magnetometer data and model are converted to and presented in spherical KRTP coordinates.

Figures 2 and 3 show two examples of aperiodic waves detected in the magnetometer data (black) fitted with the local model (red). Figure 2 shows a wave that causes Cassini to encounter the current sheet, with little in the way of variation in B_θ, this example has a MSE value of 0.06 nT. Figure 3 shows a wave that displaces the current sheet towards Cassini, but Cassini does not encounter it. This example shows a swept forward field in B_ϕ and B_r, along with variations in B_θ. This example has an MSE value of 0.05 nT^2.

Uncertainties in the values of the fitted parameters are extracted from the covariance matrix output of the non-linear least squares fitting, where the standard deviation of the fitted parameters are the square roots of the diagonal elements of the matrix. The percentage uncertainties for a successful fit lie between 1-5% for current sheet properties and 1-10% for wave parameters. The uncertainties are related to the multi-parameter χ^2 space which is related to the previously mentioned MSE, both of which are measurements from goodness of fit.

For example, we can plot the 2-dimensional χ^2 space for only the two wave numbers to ascertain if the fitting for the wave parameters is successful. A successful fit will show the final values in a unique local minimum (dark blue area) which is not associated with noise. This parameter space is formed by calculating the χ^2 value for each k_x and k_y values while all the other parameters remain constant. Figure 4 shows an example of this space, we see that the model has placed the values (red dot) in a low area of χ^2 however, there are other possibilities, these other possibilities may later reduce when including the χ^2 space of the other variables. The model gives a χ^2 value of 2.33, which is smaller than the majority of the 'blue valley' which give χ^2 values of around 10 to 50.

5 Results

Firstly, we explore results on the properties and structure of the current sheet that appear in the equations for the modified Harris current sheet (1, 2, 3). Figures 5, 6, and 7 show the azimuthal lobe field component, B_{y0}, mean scale height, H, and offset from the equatorial plane, z_0, respectively, projected into the X-Y plane of the KSM coordinate system. This overview plots all values of a specified parameter with respect to the position of Cassini during the event. Each box shows the mean of the parameter for the number of events that occur within it. The mean is weighted by the inverse of the MSE for each event, allowing for better fits to more strongly influence the mean.

Below the overview plot, the sector plots (b-e) show the relationship of the parameter of interest with radial distance in different local time sectors. 'Night' refers to 21:00 to 03:00 SLT (Saturn Local Time), 'Morning' refers to 03:00 to 09:00 SLT, 'Noon' refers to 09:00 to 15:00 SLT and 'Evening' refers to 15:00 to 21:00 SLT. Additionally, each point on the plots has a color associated with the revolution number of Cassini, which allows for temporal differences to also be viewed. Early Cassini orbits in 2005 are colored blue, whereas late orbits in 2012 are colored yellow.

If a correlation coefficient of more than 0.25 is found for any of the sectors, a linear fit shows the increase or decrease of parameter of interest with radial distance. The uncertainties in the linear fitting parameters shown as dashed lines either side of the fit. This linear fit is also weighted by the inverse of the MSE values for each event, so events with better fits will more strongly determine the linear fit.

We find that the lobe values of the magnetic field components with radial distance have an expected decrease. Negative values of B_{y0} are most common in the night, morning and noon sectors, relating to the sweptback features of the field. Positive values of B_{y0} are only found near the post midday flank of the magnetosphere, the area most commonly found to have swept forward field lines, all shown in figure 5.

The scale height of the overall current sheet is found by calculating the geometric mean of H_x and H_y, the two scale heights fitted are usually within uncertainties of each other for good fits. Figure 6 shows that the scale height increases from $2R_S$ to $6R_S$ as it approaches the magnetopause in the morning sector, and increases from $1R_S$ to $5R_S$ in the night sector. The evening and noon sectors show little or no correlation with radial distance.

The value of z_0 varies radially, azimuthally and with time due to the seasonal bowl shape of the current sheet discussed in section 3. Figure 7 shows increases in the morning and night sectors with increasing radial distance.

We now move onto the wave parameters, amplitude, k_x, k_y, ω and Φ_0. Most parameters show little spatial variation within Saturn's magnetosphere, but most have a large range of values. For example, angular frequency ω has a median of 0.007 s^{-1} with an interquartile range of 0.007 s^{-1}.

One parameter that does exhibit considerable variation in radial distance and local time is the wave amplitude. Figure 8 shows the spatial distribution of amplitude around Saturn. The wave amplitude becomes increasingly negative with radial distance in the morning and night sectors, from $-1R_S$ to $-2R_S$. A negative amplitude is associated with the current sheet moving to a negative position in z as an aperiodic wave passes.

Wave numbers k_x and k_y can be used to find the direction that a wave is propagating along the current sheet. Figure 9 gives an overview of the direction of propagation of all fitted waves. Again each section is split into SLT sectors as described previously, and then divided into three radial distance groups: inner ($< 20R_S$), middle ($20 - 40R_S$) and outer ($> 40R_S$). The red curve in each subplot shows an estimate of the probability distribution function for the wave propagation direction, produced by kernel smoothing. These are produced from a superposition of normal distributions with the mean of the angle of propagation and its standard deviation of the uncertainty on the angle. The angle of propagation is calculated using k_x and k_y, with respect to the Saturn-Sun line (0°), and its uncertainty is propagated through from the uncertainties on k_x and k_y. The bottom left plot in figure 9 shows the key and describes the direction of which waves in the specified area are propagating. The probability distribution for the wave that has equal probability of propagating in any direction is shown as the black circle.

All sectors and radial distances, apart from the noon sector, have statistically skewed probability distributions, skewed towards outwards radial propagation and slight azimuthal propagation in the direction of corotation. This means that in the evening sector the distribution is skewed dusk-wards, in the night sector the distribution is skewed anti-sunwards and in the morning sector the distribution is skewed dawn-wards. This measure of statistical skewness is tested against the null hypothesis of an isotropic probability distribution using the cumulative distribution function. This function uses the χ^2 value of the null hypothesis and the statistical distribution of the direction of propagation to find the probability that it could agree with the null hypothesis.The evening, night, and morning sectors all have skewed distributions that are statistically significant at the 1% level. Concluding that these sectors are all significantly skewed. The noon sector is not statistically significant at the 1% or 10% levels and so we conclude that there is no preferred wave propagation direction in the noon sector.

6 Discussion

The scale height of the current sheet was found to increase in the morning and noon sectors from $2R_S$ to $6R_S$ and $5R_S$ respectively. It is important to note that this scale height is for the magnetic field, and does not include analysis from plasma data, hence it is not directly comparable to thickness measurements made using plasma data. However the two are correlated and similar trends should be present in both magnetic and plasma data.Further discussion on this topic can be found in *Sergis et al.* [2009] and *Sergis et al.* [2011].

At Saturn, with the use of highly inclined revolutions of Cassini, *Kellett et al.* [2009] and *Kidder et al.* [2009] previously found that the vertical distribution of plasma at the current sheet extends from $1.5-2.5R_S$ in half-thickness. *Giampieri et al.* [2004] use a ring current model from *Connerney et al.* [1983] to conclude from Voyager and Pioneer flybys that the current sheet thickness increases with radial distance. *Carbary et al.* [2012] show a scale height of $1.5R_S$ using magnetometer data. The scale height result is similar to that found in the Jovian magnetosphere where *Khurana and Kivelson* [1989] have shown that the half-width of the plasma sheet grows from $4R_J$ at $20R_J$ to $7.5R_J$ at $100R_J$.

Use of a modified Harris current sheet to model the current sheet allows fitting of the z_0 value. This variable represents the distance that the current sheet is displaced along the z-axis from the equator due to other processes before the aperiodic wave passes. We assume that this value of z_0 is constant during over the period of the wave, such that the period is much shorter than the previously discussed known distortions such as the bowl and flapping waves. We find that the revolutions of Cassini that occur before 2009 (Saturn equinox) give a value of positive z_0. These revolutions occur mainly within the morning and night sectors, and during this time we would expect the current sheet to be pushed upwards into a bowl shape [*Arridge et al.*, 2008a]. Conversely, the evening and noon sector revolutions mainly occur after equinox, and so the opposite is true, z_0 is found to be negative and the current sheet is pushed below the rotational equator. Additionally, we find that there is an increase in the absolute values of z-axis offset z_0 in each local time sector with radial distance, showing that the current sheet is taking the shape of a bowl.

Wave numbers found from the fitting of a Gaussian pulse wave function to magnetometer data are used to find the propagation direction. We find that in each local time sector and radial distance bin, excluding the noon sector, the probability distributions show that waves propagate radially outwards and azimuthally in the direction of corotation. In the noon sector we find that, with lower numbers of events occurring within each bin, the distributions have more than one primary direction. Inwards of $20R_S$ we see a bi-directional distribution with a majority travelling inwards. This distribution may be due to magnetopause compression and expansion causing waves to travel from the magnetopause inwards, giving a link between solar wind conditions and aperiodic waves near the nose of the magnetosphere [e.g. *Arridge et al.* [2006], *Clarke et al.* [2006] & *Kanani et al.* [2010]]. Other sources of aperiodic waves may originate from reconnection within the tail region, where waves are induced by an explosive reconnection event and travel away from the reconnection site [*Arridge et al.*, 2016]. This may account for tail-ward waves, but would also induce planet-ward travelling waves as well, perhaps due to dipolarizations travelling planet-ward.

For the waves to be travelling radially away from the planet, a source of waves must be found in the inner dipolar magnetosphere or in the planet itself. Enhancement of the ring current may induce a large enough perturbation of magnetic field to produce an aperiodic wave [*Bunce et al.*, 2007; *Kellett et al.*, 2011]. We also suggest that centrifugal interchange processes may also provide a sufficient disturbance to the system in the inner magnetosphere to produce aperiodic waves travelling radially outwards, these processes have been studied both observationally by [e.g. *Burch et al.*, 2005; *Mauk et al.*, 2005] and through numerical simulation [e.g. *Kidder et al.*, 2009].

The next radially varying parameter is the amplitude of the waves. We find that in the morning and night sectors the amplitude increases from $1R_S$ to $2R_S$ over radial distances from $15R_S$ to $50R_S$. To test that this behavior is not a viewing bias introduced by the vertical separation of Cassini from the current sheet in the outer magnetosphere, we checked the coverage of in situ measurements and z_0 fitting. Cassini covers a range from $-10R_S$ to $10R_S$ in z, which is greater than the largest amplitudes found and so will be close enough to the current sheet at large radial distances to be able to see the smaller amplitude waves, but does not. This was tested by considering the position of Cassini subtracted from the position of current sheet in z against amplitude, of which there is no correlation. We may conclude that the lack of smaller amplitude waves at larger radial distances must be caused by the amplitude increasing due to a decrease in density and is not a viewing bias caused by the distance of the current sheet from Cassini.

Having ruled out an observer bias, we now seek a physical interpretation for the increasing amplitude. To conceptually understand the origin of the increasing amplitude, we use a physical analogy of a wave on a string or a wave in water and draw a comparison with water shoaling. The energy of the wave is related to the linear mass density, the frequency of the wave and the amplitude of the wave. Energy of the wave must remain constant, and so if the linear mass density is decreasing [*Arridge et al.*, 2011] either the amplitude or frequency of the wave must change. We measured no radial dependance on frequency, but a increasing trend with radial distance in amplitude, hence we suggest that the amplitude increase is due to the decrease in plasma density.

An underlying assumption of our model is that the wave can be described by a Gaussian pulse. However, the wave could be sinusoidally shaped, perhaps with a time-dependent amplitude. If Cassini is below the current sheet it will only view wave motion in the negative z direction as motions in the positive z direction will be invisible, or at least damped, by the asymptotic behavior of the hyperbolic tangent function in the modified Harris current sheet. This wave shape can be simulated by a Gaussian differential wave function (the differential of the Gaussian pulse wave function described previously) using the same process applied in section 4. We find that the Gaussian differential wave function fits some of the magnetometer data, however it gives a higher MSE and higher uncertainties on parameters that are found. On events where both waves fit the magnetometer data, the parameters are comparable within uncertainties. Thus we conclude that the Gaussian wave function is appropriate to characterise the magnetometer data. The Gaussian differential wave function also fails to fit the majority of events in the evening and noon sector.

As shown in figures 6 and 8, current sheet scale height and wave amplitude parameters in the evening and noon sectors show almost no variation with radial distance. The color scale shows what year and what number revolution Cassini detected the event on. In the morning and night sectors the majority of events are blue colored meaning that they all occur on subsequent revolutions in 2005. However, in the evening we see a larger range of revolutions over a larger time period (2007-2012) meaning that we are seeing temporal variations in addition to spatial differences. At the extreme we have the noon sector data which is only from the initial revolutions in 2005 and the final revolutions in 2012. We can see that the two time separated subsets of waves produce two different trends with radial distance.

Additionally, there are numerous lines of evidence to suggest that the dusk sector, and occasionally the noon sector, may have a thicker current sheet as summarised in figure 10 of *Arridge et al.* [2015]. This is consistent with jovian observations by *Krupp et al.* [1999]. The thin current sheet approximation, therefore, may not be valid for a number of events, or may provide an additional source of error for events on the dusk flanks of the magnetosphere and leads to larger uncertainties. A future analysis of the evening and noon sectors should take into account the temporal differences,assess whether the thin current sheet approximation is valid, and plot singular spacecraft orbits to decipher a correlation between a specified parameter and radial distance, if there is one present.

7 Summary

Cassini magnetometer data was surveyed for short duration aperiodic waves in Saturn's magnetosphere and a catalogue of 1461 events were found in data from January 2005 to December 2012. Assuming wave-like perturbations that could be adequately modeled by a Gaussian wave pulse, a local current sheet model was constructed and fitted to the data to estimate current sheet, magnetic field, and wave properties.

The local current sheet model consisted of a Harris current sheet for the radial and azimuthal components of the magnetic field and a constant normal component. This model was then deformed by a Gaussian wave pulse using the general deformation technique [*Tsyganenko*, 1998] which imposes $\nabla \cdot \mathbf{B} = 0$. This model was fitted to these events using an automated technique which resulted in 742 wave events having a good fit to the data.

Use of the Harris current sheet allows for current sheet and magnetic field parameters to be fitted to magnetometer data, we find that a) lobe magnetic field values showed a decrease with radial distance, as expected; b) the current sheet scale height increased with radial distance in the morning and night sectors, consistent with previous studies; c) the stationary offset of the current sheet from the equatorial plane was fully consistent with seasonal changes in the position of the bowl-shaped current sheet [*Arridge et al.*, 2008a].

Wave properties from the Gaussian wave function showed that waves were most often radially propagating outwards from the planet and toward the direction of corotation, arguing that a source of the waves must lie in the inner magnetosphere. A statistically significant single propagation direction in the noon sector was not found. This result was interpreted as evidence that multiple sources of waves are present in the noon sector. Sources such as compression and expansion of the magnetopause may cause waves to travel inwards away from the magnetopause, in addition to the aforementioned inner magnetospheric source. Although we speculated that tail reconnection may drive both inward and outward propagating waves (by analogy with results from the terrestrial magnetosphere), we argued that perturbations associated with the centrifugal interchange instability may provide an inner magnetospheric source for waves propagating radially outward.

The wave amplitude was found to increase with radial distance. An observer bias was ruled out and so this finding was interpreted as being due to the conservation of wave energy in an environment where the plasma density and magnetic field strength were decreasing.We find a range of angular frequencies, ω, from 0.0005 to 0.0750 s^{-1} which does not show any variation with local time or radial distance.

Further work on these events includes a) case studies in order to understand unusual events, for example where multiple current sheet encounters are found which may be better fitted by a sinusoidal wave function as well as singular events which may fit a different wave profile; b) incorporating plasma data into case studies or fits; c) numerical studies on the wave modes in order to better understand the origin and propagation of these waves.

Acknowledgments

CJM was funded by a Faculty of Science and Technology studentship from Lancaster University. CSA was funded by a Royal Society Research Fellowship. CJM would like to acknowledge useful discussions and comments from Sarah Badman and Licia Ray. Cassini MAG data used in this study may be obtained from the Planetary Data System (http://pds.nasa.gov/).

References

Andrews, D.J., Coates, A.J., Cowley, S.W.H., Dougherty, M.K., Lamy, L., Provan, G. and Zarka, P., (2010) Magnetospheric period oscillations at Saturn: Comparison of equatorial and high latitude magnetic field periods with north and south Saturn kilometric radiation periods. *Journal of Geophysical Research: Space Physics 115*(A12).

Arridge, C.S., Achilleos, N., Dougherty, M.K., Khurana, K.K. and Russell, C.T., (2006). Modeling the size and shape of Saturn's magnetopause with variable dynamic pressure. *Journal of Geophysical Research: Space Physics*, *111*(A11).

Arridge, C. S., Russell, C. T., Khurana, K. K., Achilleos, N., Andrï£¡, N., Rymer, A. M., Dougherty, M. K., Coates, A. J., (2007). Mass of Saturn's magnetodisc: Cassini observations, *Geophysical Research Letters*, *34*(A11), 8779–8789.

Arridge, C.S., Khurana, K.K., Russell, C.T., Southwood, D.J., Achilleos, N., Dougherty, M.K., Coates, A.J. and Leinweber, H.K., (2008a). Warping of Saturn's magnetospheric and magnetotail current sheets, *Journal of Geophysical Research: Space Physics*, *113*(A8), 2156–2202.

Arridge, C.S., Russell, C.T., Khurana, K.K., Achilleos, N., Cowley, S.W.H., Dougherty, M.K., Southwood, D.J. and Bunce, E.J., (2008b) Saturn's magnetodisc current sheet. *Journal of Geophysical Research: Space Physics*, *113*(A4).

Arridge, C. S., André, N., Khurana, K. K., Russell, C. T., Cowley, S. W. H., Provan, G., Andrews, D. J., Jackman, C. M., Coates, A. J., Sittler, E. C., Dougherty, M. K., Young, D. T. (2011) Periodic motion of Saturn's nightside plasma sheet *Journal of Geophysical Research*, *116*.

Arridge, C. S., Kane, M. , Sergis, N., Khurana, K. K., Jackman, C. J., (2015) Sources of local time asymmetries in magnetodiscs *Space Science Reviews*, *187*, 301–333.

Arridge, C.S., Eastwood, J.P., Jackman, C.M., Poh, G.K., Slavin, J.A., Thomsen, M.F., André, N., Jia, X., Kidder, A., Lamy, L. and Radioti, A., (2015). Cassini in situ observations of long-duration magnetic reconnection in Saturn's magnetotail. *Nature Physics*.

Bunce, E.J., Cowley, S.W.H., Alexeev, I.I., Arridge, C.S., Dougherty, M.K., Nichols, J.D. and Russell, C.T., (2007) Cassini observations of the variation of Saturn's ring current parameters with system size. *Journal of Geophysical Research: Space Physics*, *112*(A10) 2156–2202.

Burch, J.L., Goldstein, J., Hill, T.W., Young, D.T., Crary, F.J., Coates, A.J., Andre, N., Kurth, W.S. and Sittler Jr, E.C., (2005) Space Sciences-Special Section: Saturn's Magnetosphere: First Results From Cassini-L14SO2-Properties of local plasma injections in Saturn's magnetosphere. *Geophysical Research Letters*, *32*(14).

Carbary, J.F., Achilleos, N. and Arridge, C.S., 2012. Statistical ring current of Saturn. *Journal of Geophysical Research: Space Physics*, *117*(A6).

Clarke, K.E., André, N., Andrews, D.J., Coates, A.J., Cowley, S.W.H., Dougherty, M.K., Lewis, G.R., McAndrews, H.J., Nichols, J.D., Robinson, T.R. and Wright, D.M., 2006. Cassini observations of planetary?period oscillations of Saturn's magnetopause. *Geophysical research letters*, *33*(23).

Connerney, J. E. P., Acuña, M. H., Ness, N. F.,(1983). Currents in Saturn's magnetosphere, *Journal of Geophysical Research: Space Physics*, *88*(A11), 8779–8789.

Dougherty, M.K., Kellock, S., Southwood, D.J., Balogh, A., Smith, E.J., Tsurutani, B.T., Gerlach, B., Glassmeier, K.H., Gleim, F., Russell, C.T. and Erdos, G., Neubauer F. M., Cowley S. W. H., (2004), The Cassini Magnetic Field Investigation, *Space Science Reviews*, *114*(1), 331–383.

Felici, M., Arridge, C.S., Coates, A.J., Badman, S.V., Dougherty, M.K., Jackman, C.M., Kurth, W.S., Melin, H., Mitchell, D.G., Reisenfeld, D.B. and Sergis, N., (2016). Cassini observations of ionospheric plasma in Saturn's magnetotail lobes. *Journal of Geophysical Research: Space Physics*, *121*(1), 338-357.

Giampieri, G., Dougherty, M.K.,(2004). Modelling of the ring current in Saturn's magnetosphere, *Annales Geophysicae*, *22*, 653–659.

Harris, E. G., (1962). On a plasma sheath separating regions of oppositely directed magnetic field, *Il Nuovo Cimento (1955-1965)*, *23*(1), 115–121.

Jia, X. and Kivelson, M.G., (2012). Driving Saturn's magnetospheric periodicities from the upper atmosphere/ionosphere: Magnetotail response to dual sources. *Journal of Geophysical Research:Space Physics*, *117*(11).

Jurac, S., McGrath, M.A., Johnson, R.E., Richardson, J.D., Vasyliunas, V.M. and Eviatar, A., 2002. Saturn: Search for a missing water source. *Geophysical research letters*, *29*(24).

Kanani, S.J., Arridge, C.S., Jones, G.H., Fazakerley, A.N., McAndrews, H.J., Sergis, N., Krimigis, S.M., Dougherty, M.K., Coates, A.J., Young, D.T. and Hansen, K.C., (2010). A new form of Saturn's magnetopause using a dynamic pressure balance model, based on in situ, multi?instrument Cassini measurements. *Journal of Geophysical Research: Space Physics*, *115*(A6).

Kellett, S., Bunce, E. J., Coates, A. J., Cowley, S. W. H., (2009). Thickness of Saturn's ring current determined from north-south Cassini passes through the current layer, *Journal of Geophysical Research*, *114*(A4),.

Kellett, S., Arridge, C.S., Bunce, E.J., Coates, A.J., Cowley, S.W.H., Dougherty, M.K., Persoon, A.M., Sergis, N. and Wilson, R.J., (2011). Saturn's ring current: Local time dependence and temporal variability. *Journal of Geophysical Research: Space Physics*, *116*(A5).

Khurana, K.K., Kivelson, M.G.,(1989). On Jovian Plasma Sheet Structure, *Journal of Geophysical Research*, *94*(A9), 11,791–11,803.

Kidder, A., Winglee, R. M., Harnett, E. M., (2009). Regulation of the centrifugal interchange cycle in Saturn's inner magnetosphere, *Journal of Geophysical Research: Space Physics*, *114*(A2),.

Krupp, N., Dougherty, M. K., Woch, J., Seidel, R., Keppler, E., (1999). Energetic particles in the duskside Jovian magnetosphere, *Geophysical Research Letters*, *34*(A11), 8779–8789.

Mauk, B.H., Saur, J., Mitchell, D.G., Roelof, E.C., Brandt, P.C., Armstrong, T.P., Hamilton, D.C., Krimigis, S.M., Krupp, N., Livi, S.A. and Manweiler, J.W., (2005). Energetic particle injections in Saturn's magnetosphere. *Geophysical research letters*, *32*(14).

Mitchell, D.G., Carbary, J.F., Bunce, E.J., Radioti, A., Badman, S.V., Pryor, W.R., Hospodarsky, G.B. and Kurth, W.S., (2016). Recurrent pulsations in Saturn?s high latitude magnetosphere. *Icarus*, *263*, pp.94-100.

Palmaerts, B., Roussos, E., Krupp, N., Kurth, W.S., Mitchell, D.G. and Yates, J.N., (2016). Statistical analysis and multi-instrument overview of the quasi-periodic 1-hour pulsations in Saturn?s outer magnetosphere. *Icarus*, *271*, pp.1-18.

Pontius, D. H., and T. W. Hill., (2006) Enceladus: A significant plasma source for Saturn's magnetosphere. *Journal of Geophysical Research: Space Physics*, *111* (A9)

Provan, G., Andrews, D. J., Arridge, C. S., Coates, A. J., Cowley, S. W. H., Cox, G., Dougherty, M. K., Jackman, C. M. (2012). Dual periodicities in planetary-period magnetic field oscillations in Saturn's tail. *Journal of Geophysical Research*, *117* A1.

Russell, C.T., Huddleston, D.E., Khurana, K.K. and Kivelson, M.G., (1999) Structure of the Jovian magnetodisk current sheet:: initial Galileo observations *Planetary and Space Science* *47*(8–9), 1101–1109.

Sergeev, V., Runov, A., Baumjohann, W., Nakamura, R., Zhang, T.L., Balogh, A., Louarnd, P., Sauvaud, J.A. and Reme, H., (2004). Orientation and propagation of current sheet oscillations., *Geophysical research letters* *31*(5), –.

Sergis, N., Krimigis, S. M.,Mitchell, D. G.,Hamilton, D. C.,Krupp, N., Mauk, B. H., Roelof, E. C., Dougherty, M. K.,, (2009).Energetic particle pressure in Saturn's magnetosphere measured with the Magnetospheric Imaging Instrument on Cassini, *Journal of Geophysical Research: Space Physics*, *114*(A2),

Sergis, N., Arridge, C. S.,Krimigis, S. M.,Mitchell, D. G.,Rymer, A. M.,Hamilton, D. C.,Krupp, N., Dougherty, M. K.,Coates, A. J., (2011). Dynamics and seasonal variations in Saturn's magnetospheric plasma sheet, as measured by Cassini, *Journal of Geophysical Research: Space Physics*, *116*(A4), 8779–8789.

Smith, E.J., Davis, L., Jones, D.E., Coleman, P.J., Colburn, D.S., Dyal, P. and Sonett, C.P., (1980). Saturn's magnetosphere and its interaction with the solar wind. *Journal of Geophysical Research: Space Physics 85*(A11), 5655–5674.

Southwood, D.J., Kivelson, M. G., (2001). A new perspective concerning the influence of the solar wind on the Jovian magnetosphere *Journal of Geophysical Research: Space Physics 106*(A4).

Thomsen, M. F., Jackman, C. M., Cowley, S. W. H., Jia, X., Kivelson, M. G. and Provan, G., (2016). 2016. Evidence for Periodic Variations in the Thickness of Saturn's Nightside Plasma Sheet, *Journal of Geophysical Research: Space Physics*, –(–), –.

Tokar, R.L., Johnson, R.E., Thomsen, M.F., Delapp, D.M., Baragiola, R.A., Francis, M.F., Reisenfeld, D.B., Fish, B.A., Young, D.T., Crary, F.J. and Coates, A.J., 2005. Cassini observations of the thermal plasma in the vicinity of Saturn's main rings and the F and G rings. *Geophysical research letters*, *32*(14).

Tsyganenko, N.A., (1998). Modeling of twisted/warped magnetospheric configurations using the general deformation method, *Journal of Geophysical Research: Space Physics*, *103*(A10), 23551–23563.

Vasyliunas, V. M., (1998). Plasma distribution and flow, *Physics of the Jovian Magnetosphere*, edited by A. Dessler, Cambridge Univ. Press, New York, chap. 11, 395 ? 453.

von Papen, M., Saur, J. and Alexandrova, O., (2014). Turbulent magnetic field fluctuations in Saturn's magnetosphere. *Journal of Geophysical Research: Space Physics*, *119*(4), pp.2797-2818.

von Papen, M. and Saur, J., (2016). Longitudinal and local time asymmetries of magnetospheric turbulence in Saturn's plasma sheet. *Journal of Geophysical Research: Space Physics*, *121*(5), pp.4119-4134.

Yates, J.N., Southwood, D.J., Dougherty, M.K., Sulaiman, A.H., Masters, A., Cowley, S.W.H., Kivelson, M.G., Chen, C.H.K., Provan, G., Mitchell, D.G. and Hospodarsky, G.B., (2016). Saturn's quasiperiodic magnetohydrodynamic waves. *Geophysical Research Letters*, *43*(21).

Figure 1. Figure showing the signature of magnetic field components (r, θ, ϕ), and the geometry of the wave as it propagates, as a purely radially propagating wave (a) passes and a purely azimuthally propagating wave (b) passes Cassini.

Figure 2. Figure showing the magnetometer data in black, and the fitted model in red for spherical magnetic field components, B_r, B_θ and B_ϕ along with the residuals. To the right, three hodograms display the relationship between the three components. This example occurred on 18th Feb 2005, at $18.7R_S$ and 5.25 SLT

Figure 3. Figure showing the magnetometer data in black, and the fitted model in red for spherical magnetic field components, B_r, B_θ and B_ϕ along with the residuals. To the right, three hodograms display the relationship between the three components. This example occurred on 10th Sept 2011, at $28.7R_S$ and 16.7 SLT

Figure 4. Figure showing the χ^2 space of the wave numbers fitted by the local model, the red dot is the best fit according to the model.

Figure 5. Figure showing spacial distribution of B_{y0} of the magnetic field during the passing of aperiodic waves. a) shows an overall view of the magnetosphere with the orbits of Rhea ($9R_S$) and Titan ($20R_S$), and a minimum and maximum magnetopause position using the magnetopause model of *Arridge et al.* [2006]. Each colored box shows the mean of the B_{y0} projected onto the equatorial (X-Y) plane in that $1R_S$ bin. Below in b), c), d) and e) show the variability of B_{y0} with radial distance in each local time segment, color-coded by Cassini Rev number as indicated by the bar on the right hand side.

Figure 6. Figure showing spacial distribution of scale height of the magnetic field during the passing of aperiodic waves. Format is the same as figure 5

Figure 7. Figure showing spacial distribution of z_0. Format is the same as figure 5

Figure 8. Figure showing spacial distribution of amplitude of aperiodic waves. Format is the same as figure 5

Figure 9. Figure showing spacial distribution of propagation direction of aperiodic waves split by SLT and radial distance. Propagation direction angle is from the Saturn-Sun line (0°). The bottom left plot shows the directions at which the plots are skewed, along with an example of an isotropically propagating distribution shown in black. Arrows are shown to guide the eye.

Figure 1.

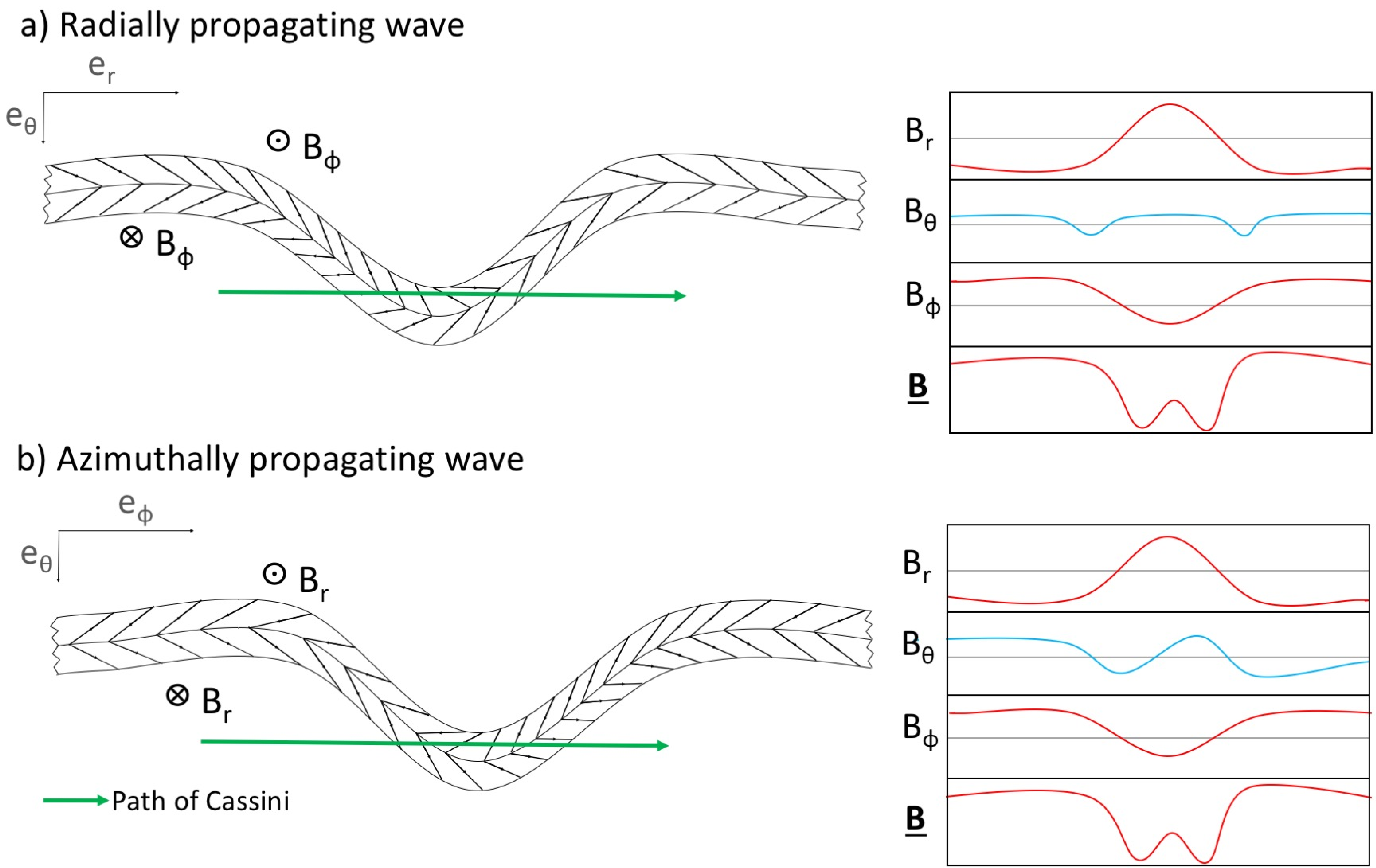
a) Radially propagating wave
e_r
e_θ
⊙ B_ϕ
⊗ B_ϕ
B_r
B_θ
B_ϕ
B
b) Azimuthally propagating wave
e_ϕ
e_θ
⊙ B_r
⊗ B_r
Path of Cassini
B_r
B_θ
B_ϕ
B

Figure 2.

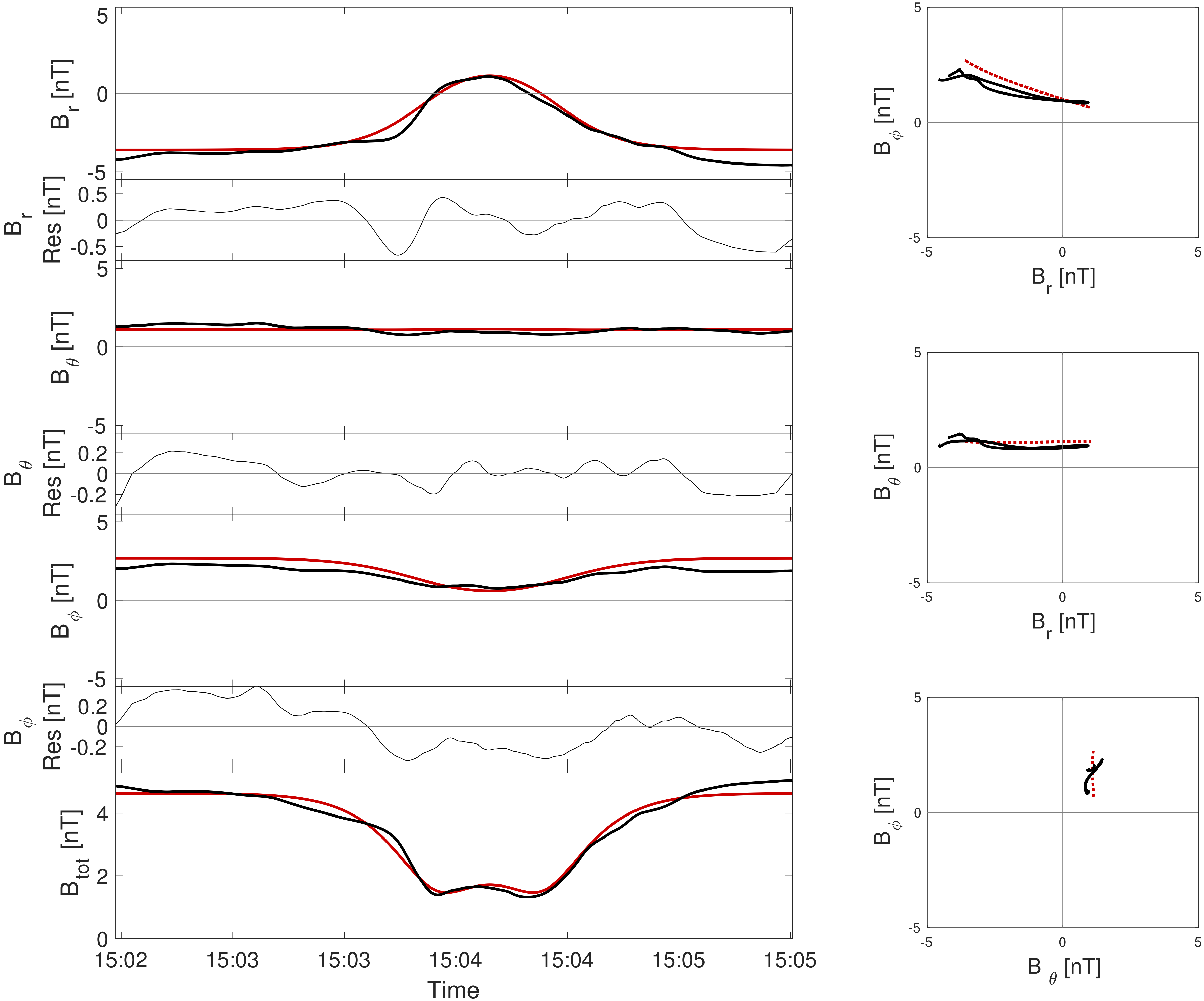

B_r [nT]
B_r Res [nT]
B_θ [nT]
B_θ Res [nT]
B_φ [nT]
B_φ Res [nT]
B_tot [nT]
15:02
15:03
15:03
15:04
15:04
15:05
15:05
Time
B_φ [nT]
B_r [nT]
B_θ [nT]
B_r [nT]
B_φ [nT]
B_θ [nT]

Figure 3.

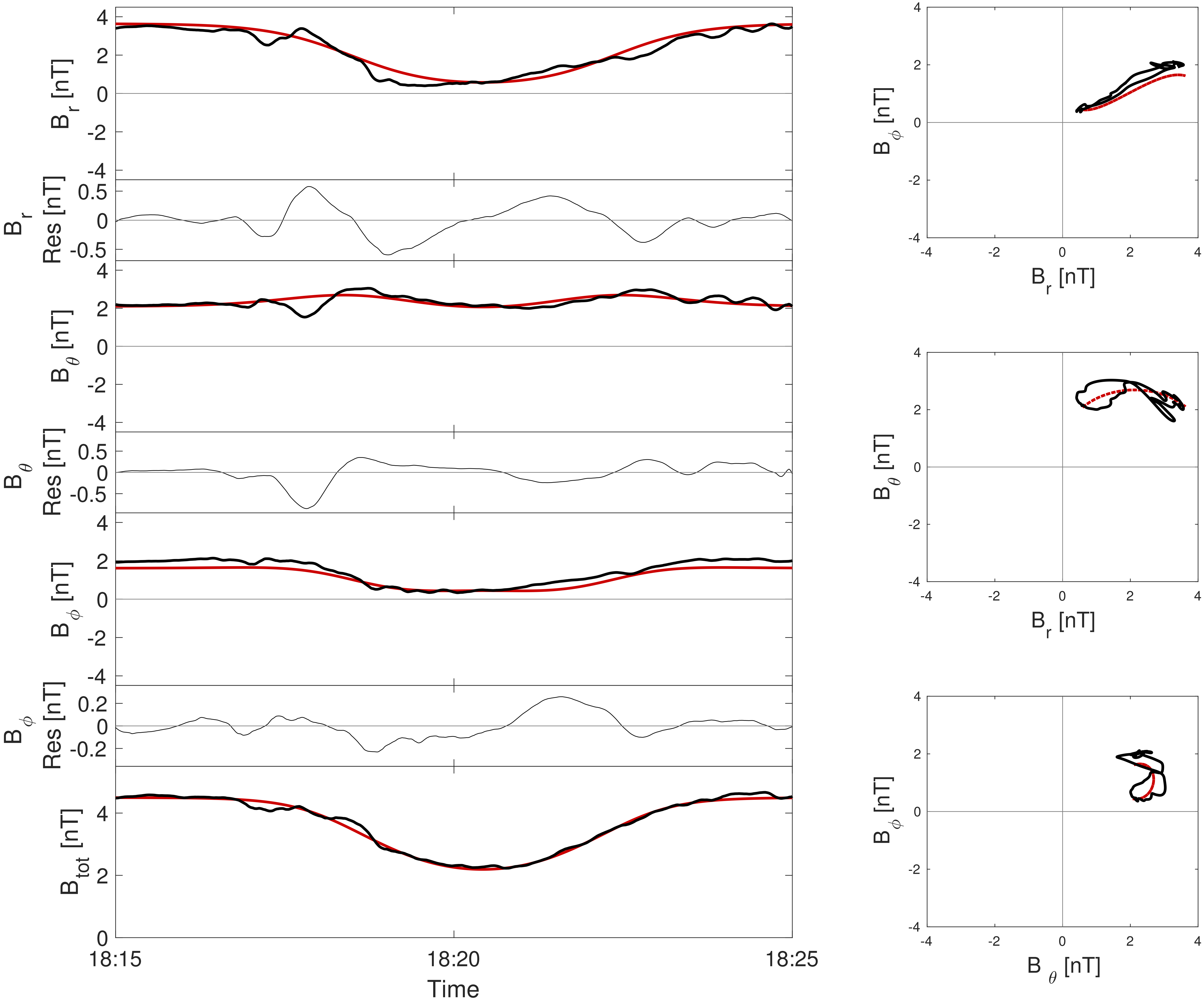

B_r [nT]
B_r Res [nT]
B_θ [nT]
B_θ Res [nT]
B_ϕ [nT]
B_ϕ Res [nT]
B_{tot} [nT]
18:15
18:20
18:25
Time
B_ϕ [nT]
B_r [nT]
B_θ [nT]
B_r [nT]
B_ϕ [nT]
B_θ [nT]

Figure 4.

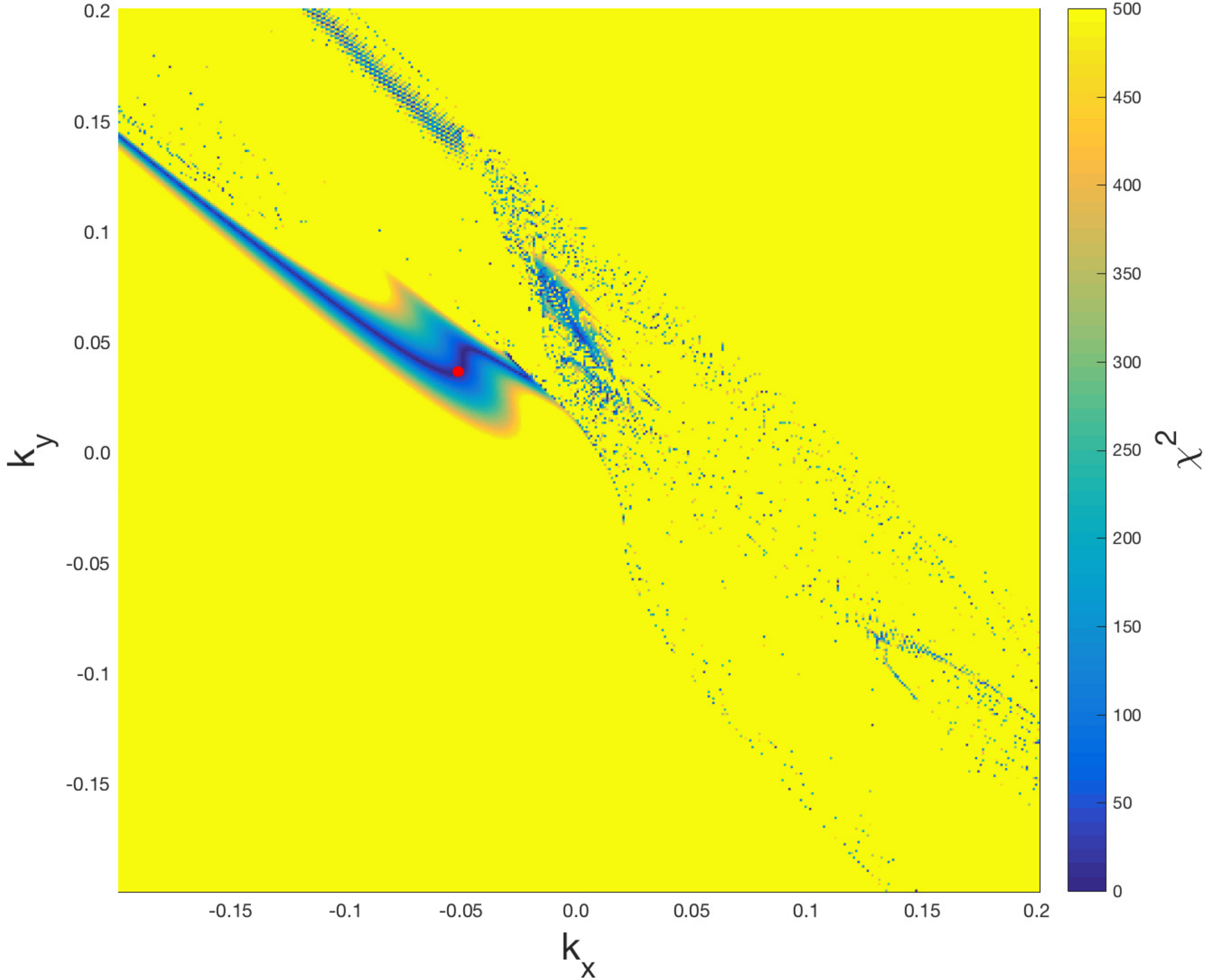

0.2
0.15
0.1
0.05
0.0
-0.05
-0.1
-0.15
k_y
-0.15
-0.1
-0.05
0.0
0.05
0.1
0.15
0.2
k_x
500
450
400
350
300
250
200
150
100
50
0
χ^2

Figure 5.

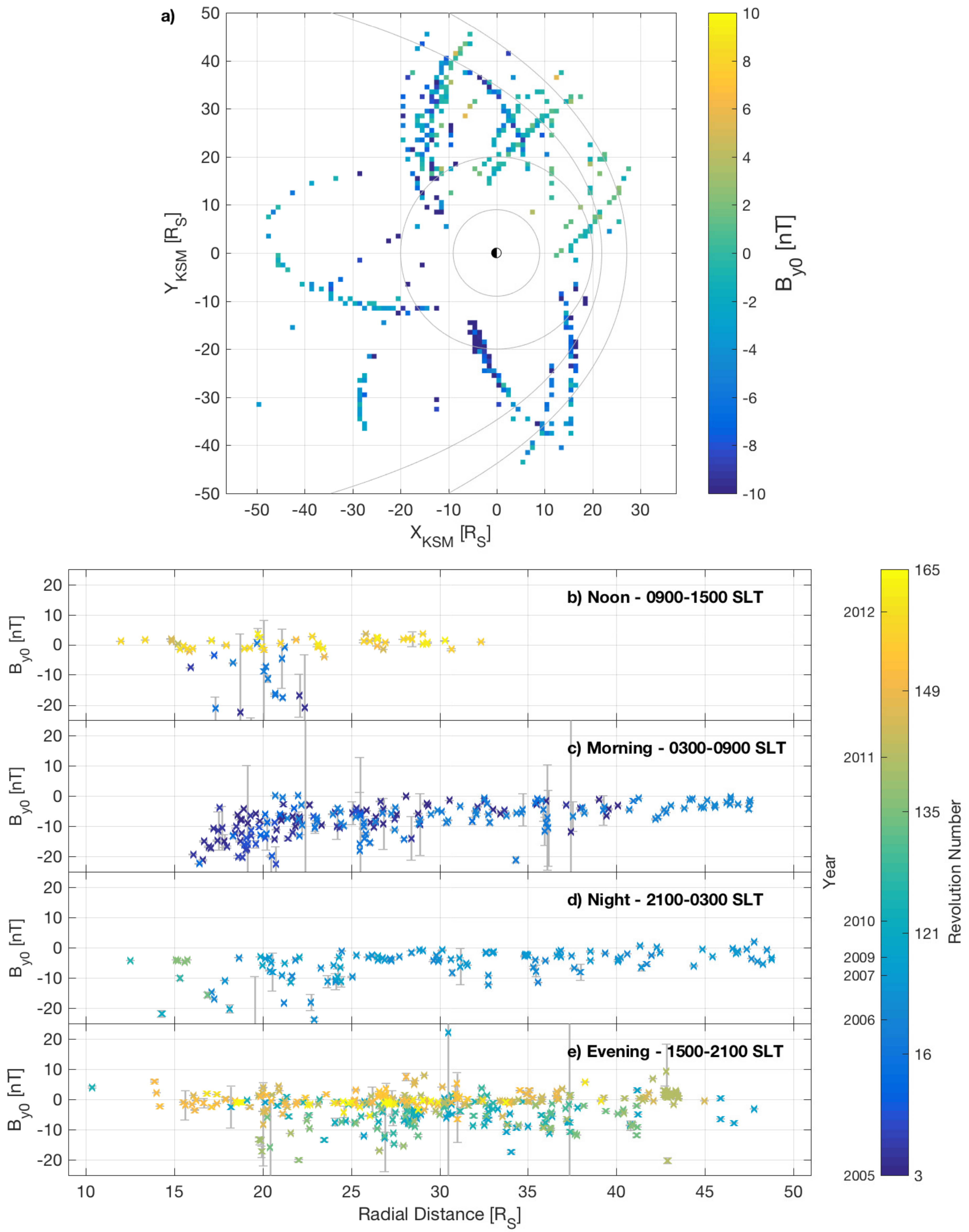

a)
Y_{KSM} [R_S]
X_{KSM} [R_S]
B_{y0} [nT]
b) Noon - 0900-1500 SLT
c) Morning - 0300-0900 SLT
d) Night - 2100-0300 SLT
e) Evening - 1500-2100 SLT
Radial Distance [R_S]
Year
Revolution Number

Figure 6.

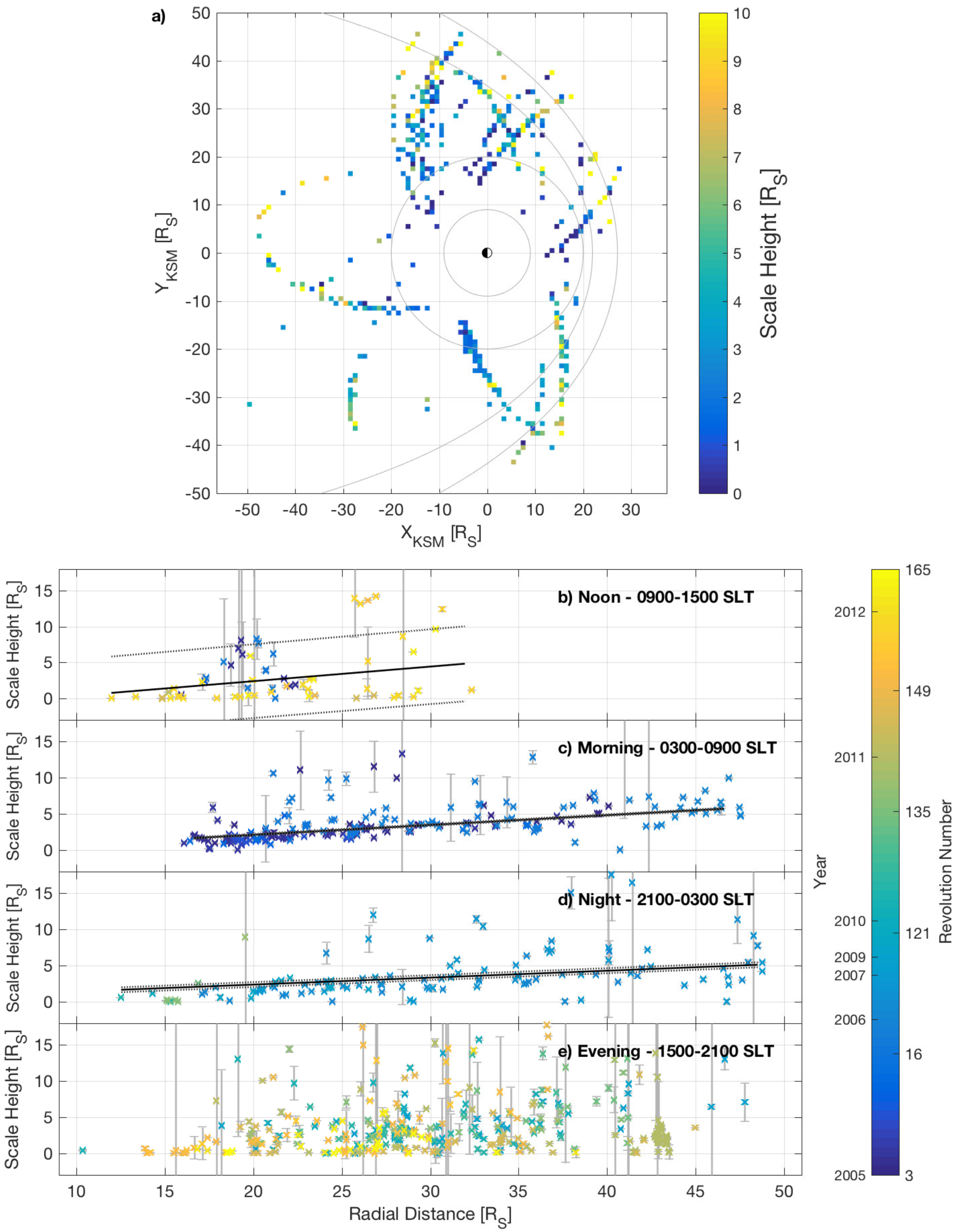

a)
Y_{KSM} [R_S]
X_{KSM} [R_S]
Scale Height [R_S]
b) Noon - 0900-1500 SLT
c) Morning - 0300-0900 SLT
d) Night - 2100-0300 SLT
e) Evening - 1500-2100 SLT
Scale Height [R_S]
Radial Distance [R_S]
Year
Revolution Number
2005
2006
2007
2009
2010
2011
2012
3
16
121
135
149
165

Figure 7.

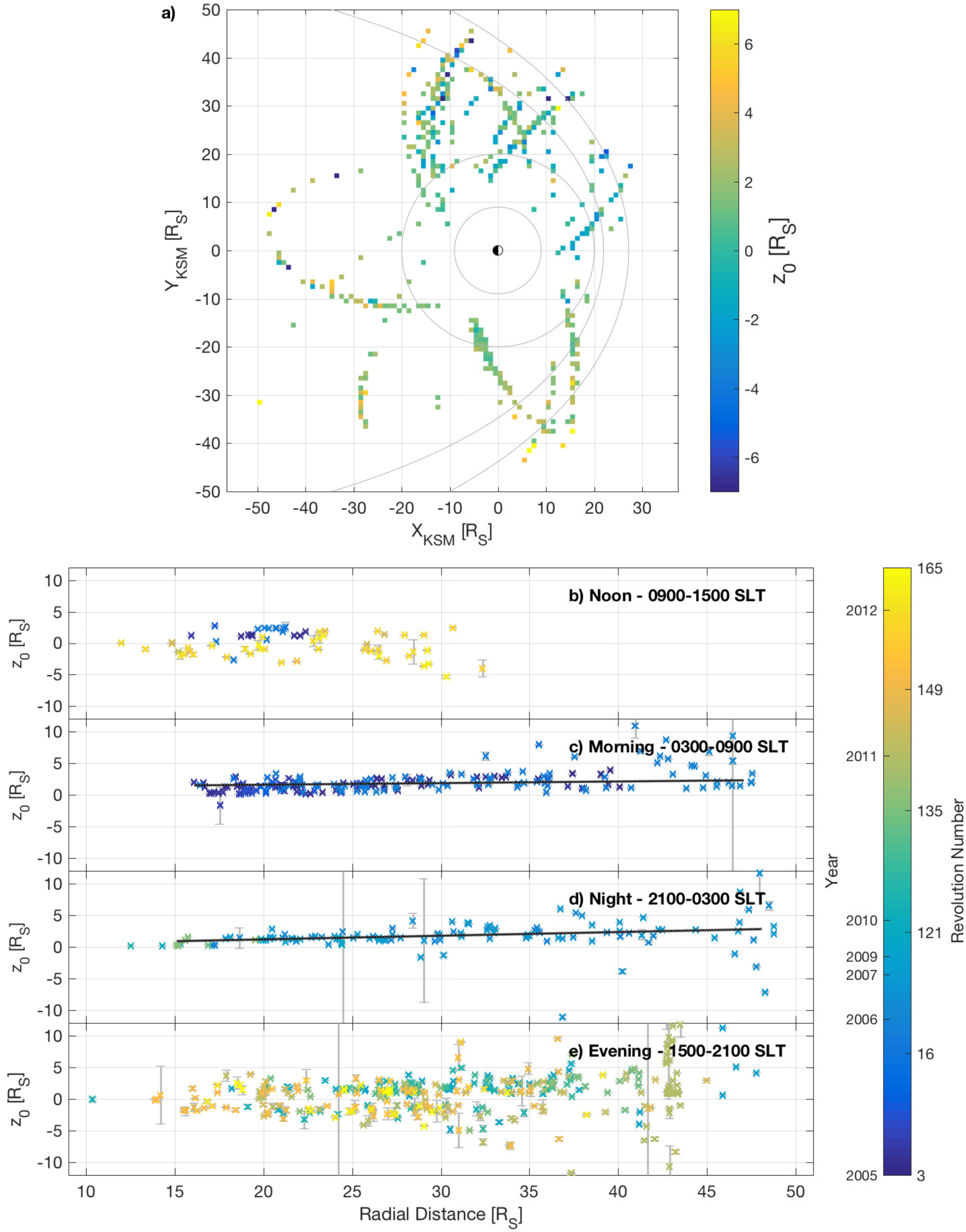

a)
Y_{KSM} [R_S]
X_{KSM} [R_S]
z_0 [R_S]
b) Noon - 0900-1500 SLT
c) Morning - 0300-0900 SLT
d) Night - 2100-0300 SLT
e) Evening - 1500-2100 SLT
z_0 [R_S]
Radial Distance [R_S]
Year
Revolution Number
2012
2011
2010
2009
2007
2006
2005
165
149
135
121
16
3

Figure 8.

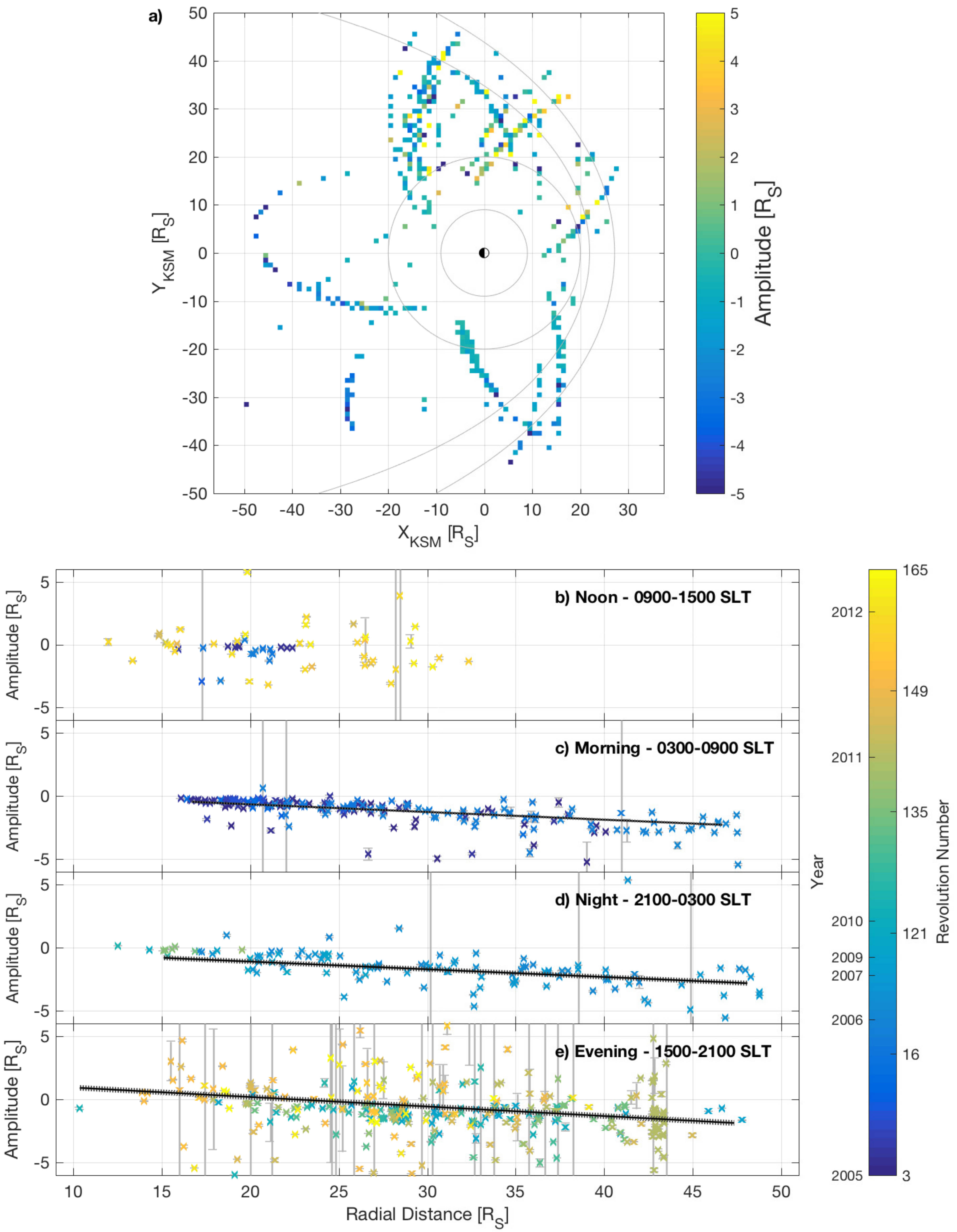
a)
Y_{KSM} [R_S]
X_{KSM} [R_S]
Amplitude [R_S]
b) Noon - 0900-1500 SLT
c) Morning - 0300-0900 SLT
d) Night - 2100-0300 SLT
e) Evening - 1500-2100 SLT
Amplitude [R_S]
Radial Distance [R_S]
Year
Revolution Number

Figure 9.

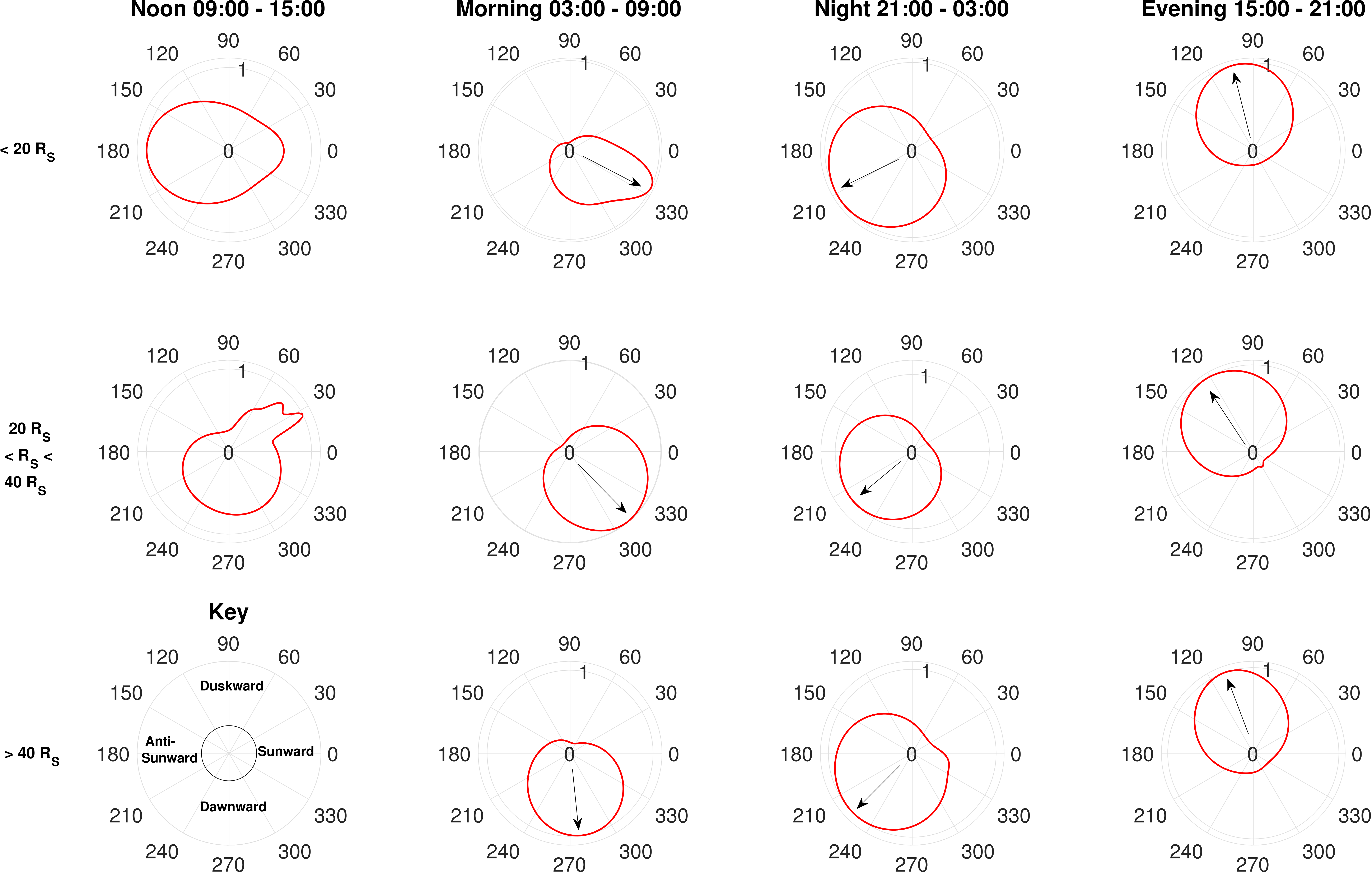

Noon 09:00 - 15:00
Morning 03:00 - 09:00
Night 21:00 - 03:00
Evening 15:00 - 21:00
< 20 R_S
20 R_S < R_S < 40 R_S
> 40 R_S
Key
Duskward
Anti-Sunward
Sunward
Dawnward